Ag−Fe_3O_4 Dimer Colloidal Nanoparticles: Synthesis and Enhancement of Magnetic Properties

Gleyguestone Lopes,[†] José M. Vargas,*[,†] Surender K. Sharma,[†] Fanny Béron,[†] Kleber R. Pirota,[†] Marcelo Knobel,[†] Carlos Rettori,[†] and Roberto D. Zysler[‡]

Instituto de Física "Gleb Wataghin", UNICAMP, Campinas-SP, 13083-970, Brazil, and Centro Atómico Bariloche, S. C. Bariloche-RN, 8400, Argentina

Received: March 14, 2010; Revised Manuscript Received: April 24, 2010

This paper describes a solution-phase route to prepare Ag−Fe_3O_4 colloidal dimer nanoparticles (NPs) with a dumbbell-like shape. Results show enhancement of the magnetic anisotropy and large coercivity that are explained through the nonzero orbital moment, m_{orb}, and the related strong spin−orbit interaction that can be induced by a lattice distortion of the Fe−O bond lengths. In particular, distortions of the octahedral sites in magnetite result in Fe 3d−O 2p mixing and O 2p to Fe 3d charge transfer which, together with crystal field effects, lifts the electronic degeneracy, leading to a nonzero m_{orb}. dc magnetization and ferromagnetic resonance were employed for analyzing the magnetic response of the reference Fe_3O_4 NPs and Ag−Fe_3O_4 dimer NPs samples, showing a very good agreement with the structural characterization.

Introduction

The understanding of the influence of surface and finite size effects on nanomaterial properties represents one of the actual cuting-edge subjects in science, from both academic and technological points of view.[1,2] Furthermore, the combination of electronic and magnetic responses through a dimer particle system allows us to study microscopically the complex and intricately interaction mechanism within the dimer structure and the possibility to tune and enhance the magnetic properties.[3−5]

In particular, metallic Ag and Au systems in the nanoscale regime exhibit striking features that are not observed in the bulk counterparts, for example, the ferromagnetism reported in Au NPs coated by protective agents, such as dodecane thiol.[6] In this case, Crespo et al.[7,8] showed that the main modification consists of the induction of lattice expansion and 5d band holes localized in the vicinity of the thiol bond through that the strong spin−orbit coupling, associated with a high local anisotropy, freezes the magnetic moment along the local easy axis and gives rise to the appearance of permanent magnetism at the nanometric scale. In magnetic ε-Fe_2O_3 NPs, Tseng et al.[9] studied the effect of the crystalline structure distortion on the Fe 3d−O 2p mixing and O 2p to Fe 3d charge transfer, which, together with crystal field effects, lifts the electronic degeneracy, leading to a nonzero m_{orb}, resulting in a moderate anisotropy, large coercivity at room temperature, and magnetoelectric effects in this material. However, because transition-metal oxides present weak spin−orbit coupling due to the so-called orbital quenching, the possible existence of orbital moments in iron oxide nanomaterials was not explored thus far.

Neglecting the surface effects, the orientation of the magnetic moment in a monodomain NP orientates itself with respect to the anisotropy axis. In the absence of an external magnetic field, the two equivalent, but opposite, orientations of the magnetic moment are separated by an energy barrier, E_B, proportional to the particle volume. The blocking temperature, T_B, corresponds to the temperature above which most of the particles are superparamagnetic, whereas below T_B, the magnetization exhibits hysteresis phenomena. In particular, magnetite (Fe_3O_4) is a common magnetic iron oxide with a cubic inverse spinel structure: oxygen forms a fcc close packing, and Fe cations occupy interstitial tetrahedral and octahedral sites.[10] Magnetite particle dispersions have been widely used as ferrofluid in, for example, rotary shaft sealing, oscillation damping, and position sensing.[11] The use of properly coated magnetite NPs in clinical medicine has also intensified. Such a suspension can interact with an external magnetic field and be positioned to a specific area, facilitating magnetic resonance imaging for medical diagnosis[12] and ac magnetic field-assisted cancer therapy.[13]

Dimer types of NPs, that is, iron oxide particles attached to metallic and nonmagnetic particles, such as silver, provide NPs' stability in solution and help in binding various biological ligands to the NPs' surface. Thus, they could be used as nanovectors for drug delivery with convenient enhancement of both optical and magnetic properties.[14,15] Therefore, the proposition of a method for designing particles with the physical properties of a Ag nanoparticle composition but with the chemistry of iron magnetite oxide would represent a major advance. Here, we describe a solution-phase route to prepare Ag−Fe_3O_4 colloidal dimer NPs. The structural and magnetic results show that the enhancement of the magnetic anisotropy and coercive field up to room temperature provides unique evidence that changes in orbital magnetization and related changes in spin−orbit coupling in the dimer compound are responsible for these facts. For this study, we have measured the dc magnetic response and the temperature dependence of the resonance field and line width of the FMR spectra.

Experimental Section

A two-step chemical method for the synthesis of Ag−Fe_3O_4 colloidal NPs was developed. All synthesis experiments were carried out using standard airless procedures and commercially available reagents. For each kind of synthesis, the prepared

* To whom correspondence should be addressed. E-mail: vargasjm@ifi.unicamp.br.
[†] Universidade Estadual de Campinas.
[‡] Centro Atómico Bariloche.

10.1021/jp102311u
Published on Web 05/14/2010

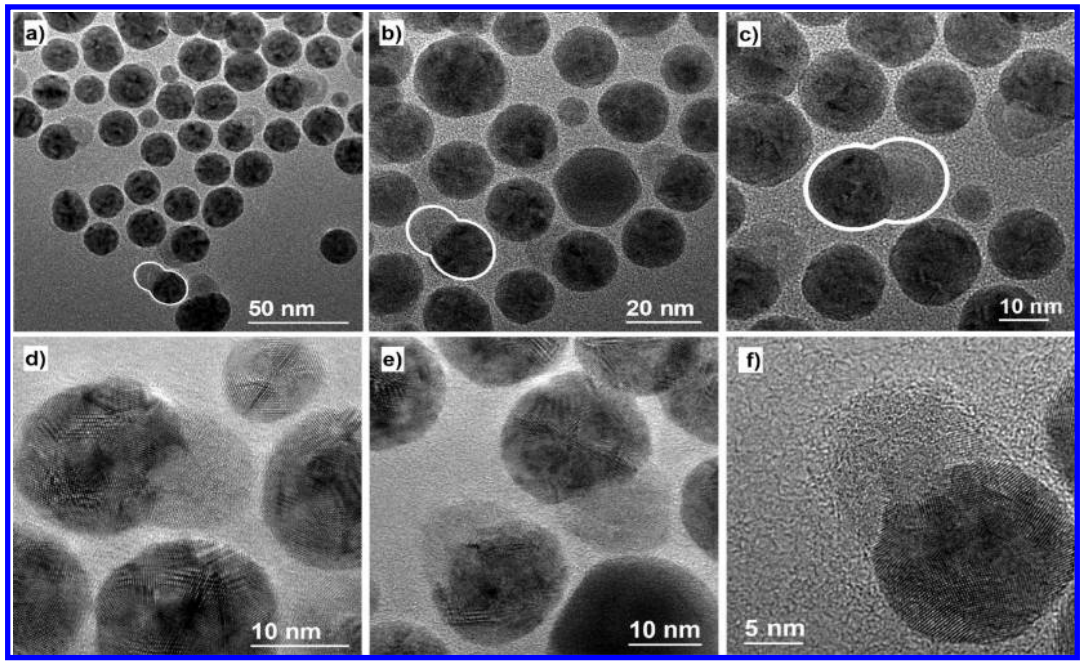

Figure 1. TEM (a−c) and high-resolution TEM (d−f) images of the Ag−Fe_3O_4 dimer NPs. The white semicircles indicate the attached particles of iron (whiter) and silver (darker).

mixture was gently heated to the final temperature of 250 °C for 40 min under an Ar gas flux. The solution was then cooled to room temperature *T*. The colloidal NPs were washed and centrifuged after adding excess ethanol. The obtained NPs were then dispersed in an adequate solvent.

Synthesis of Ag Nanoparticles. The primary reaction involves the nucleation and growth of the silver NPs with a mean size of 11.5 nm and $\sigma = 0.15$. The Ag metallic precursor ($C_{54}H_{45}NO_3P_3Ag$) was prepared from the stoichiometric amount of silver nitrate (1.1 mmol) and triphenylphosphine (3 mmol), mixed in 10 mL of warm acetonitrile. A white powder is obtained after heating at 80 °C in an inert atmosphere for 3 h. Thereafter, 10 mmol of oleyamine and 10 mmol of oleic acid were slowly added to the phenyl−ether solution of the Ag metallic precursor. This mixture was processed as described above, and the obtained Ag particles were dispersed in phenyl−ether and subsequently used as seeds. The reference sample of Ag NPs is labeled as Ag NPs sample.

Synthesis of Fe_3O_4 Nanoparticles. Magnetite NPs with a mean size of 9.0 nm and $\sigma = 0.21$, were grown by the high-temperature (250 °C) decomposition of $Fe(acac)_3$ (2 mmol) in the presence of 1,2-hexadecanediol (10 mmol) and the surfactants oleic acid (0.6 mmol) and oleylamine (0.6 mmol) in phenyl−ether, as described elsewhere.[16] The synthesized magnetite NPs were dispersed in toluene. The reference sample of Fe_3O_4 NPs is labeled as Fe_3O_4 NPs sample.

Synthesis of Ag−Fe_3O_4 Heterodimer Nanoparticles. In a typical process to obtain Ag−Fe_3O_4, 10 mL of Ag colloidal NPs in phenyl−ether (concentration of 0.05 g/mL) was added and mixed with 0.23 mmol of $Fe(acac)_3$ in the presence of 1,2-hexadecanediol (0.21 g) and the surfactants oleic acid (1.5 mmol) and oleylamine (1.5 mmol). The mixture was previously heated at 80 °C in an inert atmosphere for 40 min before undergoing the final heating/cooling steps. The obtained particles can be easily dispersed in nonpolar solvents, such as toluene or chloroform. This sample is labeled as Ag−Fe_3O_4 NPs sample.

Characterization Techniques. The particle diameters and its distribution were measured by transmission electron microscopy (TEM) (300 keV, JEM 3010 microscope) and by small-angle X-ray scattering (SAXS) in transmission mode, using synchrotron radiation ($\lambda = 1.7556$ Å), both at the Brazilian Synchrotron Light Laboratory (LNLS). For SAXS measurements, the sample was prepared in a colloidal solution of toluene at a 1:20 volume concentration. The particle composition was carried out by means of energy-dispersive spectroscopy (EDS) using a 16 nm probe, where iron and silver peaks were indexed. Samples were prepared by dropping a colloidal suspension of NPs onto a carbon-coated copper grid. The structure was determined by X-ray diffraction (XRD) (Philips, X-PERT), and the magnetic properties were measured with a SQUID (Quantum Design, MPMS XL) magnetometer. FMR spectra were measured for the toluene colloidal sample (freezing temperature ~ 180 K) in a Bruker spectrometer at $\nu = 9.5$ GHz (X band). Appropriate resonators coupled to a helium gas flux system allows us to control the temperature in the range of 4.2 K < *T* < 300 K.

Results and Discussion

Morphology and Crystallinity. Figure 1 shows typical TEM images of the Ag−Fe_3O_4 dimer NPs. The polycrystalline dimer NPs are coated by surfactant molecules, yielding a spacing of ~2 nm between them. Low-resolution images (Figure 1a−c) confirm two different contrasts in the morphology of the majority of the particles. Roughly, the profile of a particle with a homogeneous density is proportional to Z^2 and the thickness at every projected point. Therefore, the Ag particles, which have the higher *Z* compared with the Fe_3O_4 particles, are imaged as brighter dots.[4] By the shape of the particles, we can infer that, in the second synthesis step, the magnetite grows using the silver particles as pinning seeds, leading to the appearance of dimer-like particles (see HRTEM images in Figure 1d−f). A highly homogeneous log-normal distribution of particles with a mean diameter of $D = 16.0$ nm, with a standard deviation $\sigma = 0.18$, is obtained for the Ag particle seeds (dark contrast) in the Ag−Fe_3O_4 NPs sample, whereas the glued Fe_3O_4 particles (clear contrast) show a mean size between 7 to 10 nm, with a polycrystalline nature or nonpreferential crystalline orientation. Taking these values into account, SAXS experiments were

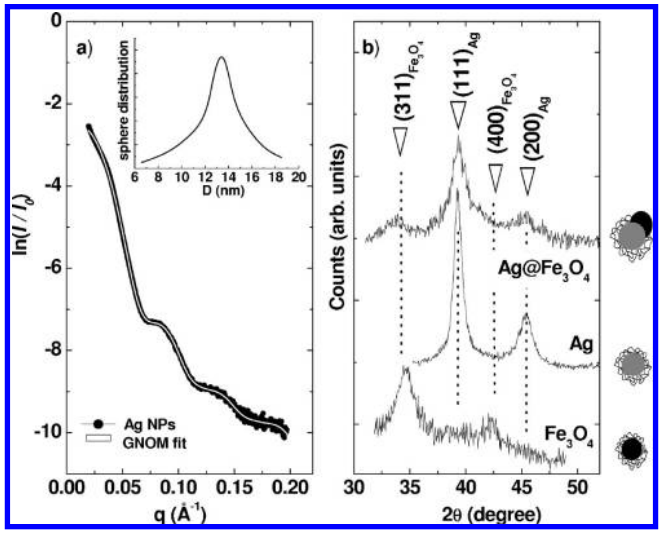

Figure 2. (a) SAXS pattern for the reference Ag NP seeds (the white line corresponds to the fitted GNOM curve considering a polydisperse system of solid spheres). The inset shows the GNOM size distribution. (b) X-ray diffraction patterns for the Ag and Fe_3O_4 reference NP samples and the Ag−Fe_3O_4 dimer NPs (the dotted lines correspond to the position of the diffraction peaks).

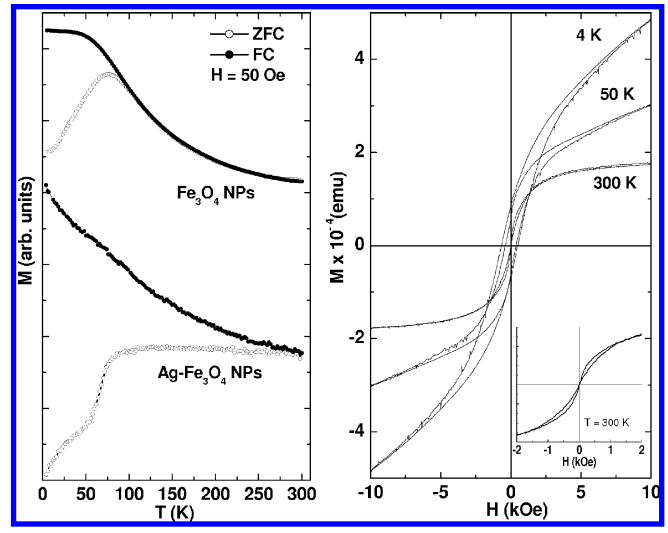

Figure 3. (a) ZFC and FC magnetizations for the Fe_3O_4 and Ag−Fe_3O_4 dimer NP samples under an applied field of 50 Oe. (b) Hysteresis loops taken at 4, 50, and 300 K (inset shows, in detail, the wasp-waist shape of the loop taken at $T = 300$ K) for the Ag−Fe_3O_4 dimer NPs.

performed to obtain a more precise understanding of the size distribution of the Ag particle seeds. Figure 2a) shows the SAXS curve for the reference Ag NPs sample along with the fit obtained using the GNOM program (considering the negligible effect of the organic-capping and polydisperse solid spheres),[17] which gives a mean size of 13.5 nm with $\sigma = 0.11$. Figure 2b) shows the XRD patterns for the Ag and Fe_3O_4 reference samples and the Ag−Fe_3O_4 NPs sample, respectively. The Ag−Fe_3O_4 pattern shows the strong contribution of the peaks indexed as Ag NPs encompassed by the very broad peaks indexed as magnetite, Fe_3O_4 (cubic phase, *Fd3m*). The detailed analysis of the peak positions and their relative intensities confirm a lattice expansion for the magnetite that has been estimated to be 2.68(7) Å, which is 4% and 6% larger than the corresponding values for the reference Fe_3O_4 sample and standard bulk (2.5314 Å), respectively. Furthermore, lattice distortion was not observed from the indexed Ag peaks in the dimer sample. Taking the full width at half-maximum (fwhm) of the most intense peak and using the Scherrer formula,[10] we have determined the effective crystalline size for the Ag (7(1) nm) and Fe_3O_4 (3(1) nm) NPs. These values are in good agreement with the HRTEM images of the Ag−Fe_3O_4 NPs sample, in which case a polycrystalline structure is observed.

dc Magnetization. Figure 3a shows the T dependence of the magnetization for the reference Fe_3O_4 and Ag−Fe_3O_4 NPs samples under zero-field-cooling (ZFC) and field-cooling (FC) conditions ($H = 50$ Oe). The shape of the ZFC−FC magnetization curves for the reference magnetite sample is the shape typically observed for weakly dipole−dipole interacting systems of randomly oriented NPs,[18] where the M_{ZFC} show a maxima at 76 K and the M_{FC} monotonically rises as T decreases, and below to 50 K, the M_{FC} is practically constant. Correspondingly, for the dimer Ag−Fe_3O_4 NPs, the M_{ZFC} curve shows clearly two contributions. At low temperatures (up to 50 K), the magnetization emerges due to the individual magnetite nanoparticles (without the attached Ag particle), and it is added to the magnetic contribution of the dimer nanoparticles leading to a very large energy barrier distribution, with blocking temperatures higher than room temperature. Concomitantly, its M_{FC} curve rises monotonically as T decreases, where the bump close to 76 K emerges due to the contribution of partially blocked magnetite nanoparticles. The irreversibility temperature, T_{irr}, is defined as the threshold temperature above which FC and ZFC curves coincide. Therefore, when the values for both Fe_3O_4 and Ag−Fe_3O_4 NPs samples are compared, the T_{irr} rises from 150 K to above room temperature; that confirms the enhancement of the magnetic anisotropy. Recently, Frey et al.[19] studied by ac susceptibility the frequency-dependent blocking temperature of dumbbell-like Au−Fe_3O_4 NPs with similar morphological characteristics. The result was fitted to two separate models in an attempt to understand the relaxation and the role of interactions present in these kinds of nanoparticle arrays, using the Nèel−Arrhenius (noninteracting single-domain NPs) and Vogel−Fulcher (weakly interacting single-domain NPs) models, respectively. The disagreement between both models and the weak accuracy in the description of the results reinforce the fact that interactions in the dumbbell-like particles are rather complex, and they cannot be accounted for by simple interparticle interactions. As mentioned by Frey and co-workers, the strong difference between both models suggests that a robust exchange type of coupling mediated by a nonmagnetic metal may be the reason for such disagreement.[19,20] Moreover, considering the same volume of the reference sample and the Fe_3O_4 part of the dimer sample, the increase in T_{irr} in the dimer NP system cannot be caused merely by dipolar interactions. As can be seen in ref 18, the strong dipolar interactions present in the powdered Fe_3O_4 sample only induce a T_{irr} shift of a few degrees (K), not comparable with the result shown in Figure 3a.

Figure 3b shows the magnetization loops for the Ag−Fe_3O_4 NPs sample at room temperature, $T = 50$ K, and $T = 4$ K (maximum applied magnetic field up to 50 kOe). At low temperature, the loops show two contributions: the high-field linear magnetic susceptibility and a ferromagnetic component. Interestingly, the magnetization curve shows a wasp-waist shape at room temperature (i.e., loop where the width narrows as the magnetization goes to zero and then opens up again).[21] Furthermore, compared with the magnetic field response of the magnetite reference sample, the enhancement of the magnetic anisotropy is evident: the reference Fe_3O_4 NPs sample presents a superparamagnetic behavior for T higher than 90 K (i.e., without a hysteretic trend), whereas the dimer system is

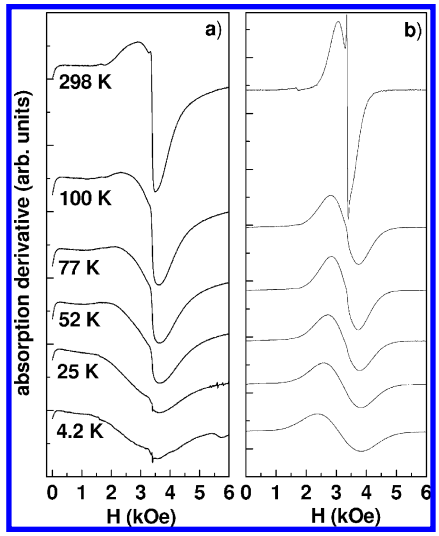

Figure 4. FMR spectra ($\nu = 9.5$ GHz) at different temperatures for the (a) Ag−Fe_3O_4 dimer and (b) reference Fe_3O_4 NPs samples.

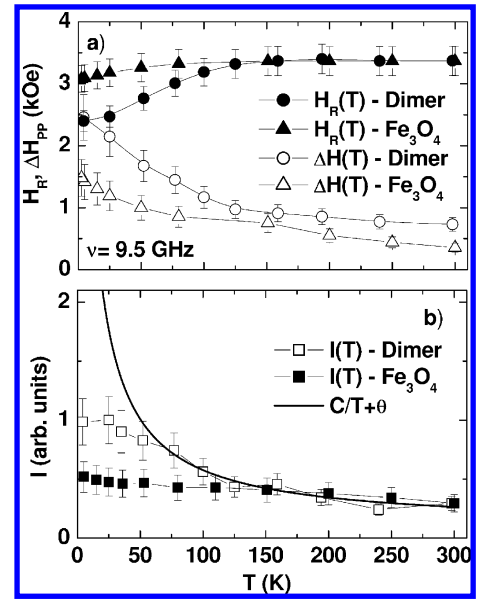

Figure 5. (a) Resonance field (H_R), line width (ΔH_{pp}), and (b) integrated intensity (I) of the FMR spectrum as a function of temperature for the reference Fe_3O_4 and Ag−Fe_3O_4 dimer NP samples. The FMR smooth line ($C/(T + \Theta)$) is extrapolated from high-T fits.

ferromagnetic up to room temperature. Moreover, the coercive field at $T = 4$ K increases from 300 Oe (Fe_3O_4) to 500 Oe (Ag−Fe_3O_4). Also, the nonsaturation magnetization of dimer nanoparticles with a high-field linear magnetic susceptibility reinforces this fact. Therefore, taking into account the morphology of the particles and the crystalline distortion of the iron oxide phase, we believe that the mechanism behind the enhancement of the magnetic anisotropy and large coercivity result from the nonzero orbital moment, m_{orb}, and the related strong spin−orbit interaction.[9,22]

FMR Experiments. Figure 4 shows the T variation of the FMR spectra in the ZFC condition for the Ag−Fe_3O_4 and reference Fe_3O_4 NPs samples. From the absorption derivative spectra, two characteristic parameters were defined: the resonant field H_0, as the point where the spectrum equals to zero, and the peak-to-peak line width ΔH_{pp}. As observed in Figure 4 and comparing with the reference sample, the broadening of the resonance spectra is evidenced for the dimer sample, where the asymmetric spectra can be described as a sum of two lines: a broad line, associated with the single-magnetic-domain contribution, and a narrow one with $\Delta H_{pp} \sim 50$ Oe, associated with the uncompensated spin contribution.[23] When the sample is cooled in a ZFC mode, the narrow line decreases steeply and the broad line shifts toward lower fields and its width increases. The integrated FMR absorption intensities, I_{FMR} (T), were calculated through the double integration of the absorption derivative spectra at each temperature. In Figure 5 are shown the T variation of ΔH_{pp}, H, and I for the Ag−FeO and reference Fe_3O_4 NPs samples. For $T < 95$ K, a drop of the resonance field coupled to the increase of ΔH_{pp} is quite noticeable (Figure 5a). These characteristics reinforce the fact of the enhancement of the effective magnetic anisotropy that can be interpreted through the very strong site-by-site local anisotropy induced in the vicinity of the interface, between Ag and Fe_3O_4. Interestingly, similar general trends were observed in the FMR spectra of FeNiB and CoNiB core−shell NPs where the strong surface anisotropy contribution dominates the magnetic response of the systems at low temperatures, which surface magnetically disordered is a consequence of the competition between the strong site-by-site anisotropy and weakened exchange interaction (both induced by the presence of defects centers viz vacancies/broken bonds at the surface).[24,25] Concomitantly, these results are in good agreement with the dc magnetization measurements, where a sharp change in the magnetization slope of the ZFC curve close to $T = 95$ K and the wasp-waist shape of the magnetization loop up to room temperature are observed, indicating the enhancement of the magnetic anisotropy.

Conclusion

In summary, we propose a new synthesis method to obtain Ag−Fe_3O_4 dimer NPs by means of a two-step chemical method. We have measured the magnetic properties of reference Fe_3O_4 NPs (9.0 nm diameter) and Ag−Fe_3O_4 dimer NPs. By means of static and dynamic measurements, we have been able to show that the Ag due to its interface with Fe_3O_4 leads the thermal stabilization of the dimer composite NPs, greater than that of the iron oxide NPs alone. Therefore, taking into account the morphology of the particles and the crystalline distortion of the iron oxide phase, we believe that the mechanism behind the enhancement of the magnetic anisotropy and large coercivity result from the nonzero orbital moment, m_{orb}, and the related strong spin−orbit interaction. In particular, distortions for octahedral sites in magnetite result in Fe 3d−O 2p mixing and O 2p to Fe 3d charge transfer which, together with crystal field effects, lifts the electronic degeneracy, leading to a nonzero m_{orb}.

Acknowledgment. TEM data were acquired at the LME-HRTEM (JEM-3010) of the Brazilian Synchrotron Light Laboratory (LNLS). Small-angle X-ray scattering data were acquired at beamline D11A-SAXS1 at LNLS. The work at UNICAMP was supported by FAPESP and CNPq, Brazil. M.K. acknowledges the John Simon Guggenheim Memorial Foundation for the Guggenheim Fellowship 2009−2010.

References and Notes

(1) Murray, C. B.; Kagan, C. R.; Bawendi, M. G. *Annu. Rev. Mater. Sci.* **2000**, *30*, 545.
(2) Sun, Y.; Xia, Y. *Science* **2002**, *298*, 2176.
(3) Li, Y.; Zhang, Q.; Nurmikko, A. V.; Sun, S. *Nano Lett.* **2005**, *5*, 1689.
(4) Yu, H.; Chen, M.; Rice, P. M.; Wang, S. X.; White, R. L.; Sun, S. *Nano Lett.* **2005**, *5*, 379.
(5) Wang, C.; Wei, Y.; Jiang, H.; Sun, S. *Nano Lett.* **2009**, *9*, 4544.
(6) Hori, H.; Yamamoto, Y.; Ywamoto, T.; Miura, T.; Teranishi, T.; Miyake, M. *Phys. Rev. B* **2004**, *69*, 174411.

(7) Crespo, P.; Litrán, R.; Rojas, T. C.; Multigner, M.; de la Fuente, J. M.; Sánchez-López, J. C.; Garcyía, M. A.; Hernando, A.; Penadés, S.; Fernández, A. *Phys. Rev. Lett.* **2004**, *93*, 087204.

(8) Crespo, P.; Garcyía, M. A.; Fernández Pinel, E.; Multigner, M.; Alcántara, D.; de la Fuente, J. M.; Penadés, S.; Hernando, A. *Phys. Rev. Lett.* **2006**, *97*, 177203.

(9) Tseng, Y. C.; Souza-Neta, N. M.; Haskel, D.; Gich, M.; Frontera, C.; Roig, A.; Veenendaal, M. V.; Nogués, J. *Phys. Rev. B* **2009**, *79*, 094404.

(10) Cornell, R. M.; Schwertmann, U. *The Iron Oxides: Structure, Properties, Reactions, Occurrence and Uses*; VCH: New York, 1996.

(11) Raj, K.; Moskowitz, R. *J. Magn. Magn. Mater.* **1990**, *85*, 233.

(12) Oswald, P.; Clement, O.; Chambon, C.; Schouman-Claeys, E.; Frija, G. *Magn. Reson. Imaging* **1997**, *15*, 1025.

(13) Jordan, A.; Scholz, R.; Wust, P.; Fahling, H.; Felix, R. *J. Magn. Magn. Mater.* **1999**, *201*, 413.

(14) Arruebo, M.; Fernandez-Pacheco, R.; Ibarra, M. R.; Santamaría, J. *Nano Today* **2007**, *2*, 23.

(15) Goya, G. F.; Grazu, V.; Ibarra, M. R. *Curr. Nanosci.* **2008**, *4*, 1.

(16) Vargas, J. M.; Zysler, R. D. *Nanotechnology* **2005**, *16*, 1474.

(17) Glatter, O.; Kratzy, O. *Small Angle X-Ray Scattering*; Academic Press Inc.: London, 1982.

(18) Vargas, J. M.; Nunes, W. C.; Socolovsk, L. M.; Knobel, M.; Zanchet, D. *Phys. Rev. B* **2005**, *72*, 184428.

(19) Frey, N. A.; Phan, M. H.; Srikanth, H.; Srinath, S.; Wang, C.; Sun, S. *J. Appl. Phys.* **2009**, *105*, 07B502.

(20) Pierce, J. P.; Torija, M. A.; Gai, Z.; Shi, J.; Schulthess, T. C.; Farnan, G. A.; Wendelken, J. F.; Plummer, E. W.; Shen, J. *Phys. Rev. Lett.* **2004**, *92*, 237201.

(21) Bennetta, L. H.; Della Torre, E. *J. Appl. Phys.* **2005**, *97*, 10E502.

(22) Desjonquères, M. C.; Barreteau, B.; Autès, G.; Spanjaard, D. *Phys. Rev. B* **2007**, *76*, 024412.

(23) Vargas, J. M.; Lima, E., Jr.; Zysler, R. D.; Duque, J. G. S.; De Biasi, E.; Knobel, M. *Eur. Phys. J. B* **2008**, *64*, 211.

(24) De Biasi, E.; Ramos, C. A.; Zysler, R. D.; Romero, H. *Phys. Rev. B* **2004**, *354*, 286.

(25) De Biasi, E.; Zysler, R. D.; Ramos, C. A.; Romero, H.; Fiorani, D. *Phys. Rev. B* **2005**, *71*, 104408.

JP102311U